Edited by Xiangyu Hu

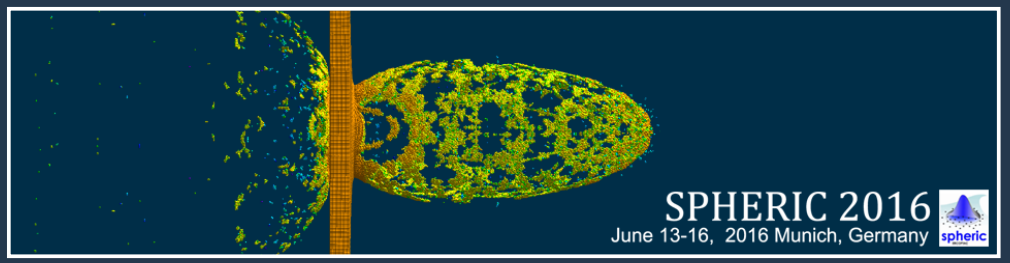

Proceedings of the 11th International SPHERIC Workshop

ISBN 9783000533587

Proceedings of the 11th International SPHERIC Workshop

Edited by Xiangyu Hu

Proceedings of the 11th International SPHERIC Workshop

June 13-16, 2016
TUM, Munich, Germany

ISBN 9783000533587

Organised by

The Institute of Aerodynamics and Fluid Mechanics,
Technical University of Munich

Edited by

Xiangyu Hu

Acknowledgement

The organisers would like to thank

SPHERIC
ERCOFTAC
ALTAIR
NVIDIA
DFG

Consistency issues on SPH energy conservation when simulating viscous flows around solid bodies

J.L. Cercos-Pita
A. Souto-Iglesias
CEHINAV, res.gr., DMFPA, ETSIN
Technical University of Madrid (UPM)
28040 Madrid, Spain
antonio.souto@upm.es

M. Antuono
A. Colagrossi
CNR-INSEAN
Marine Technology Research Institute
00128 Rome, Italy
andrea.colagrossi@cnr.it

***Abstract*—The energy conservation properties of SPH in the presence of fluid-solid interactions are investigated in this paper. Similarly to the fluid phase, the solid bodies are modeled through solid particles so that the whole solid-fluid domain can be described as a unique particle system. The pressure and velocity fields are then extended over the solid particles in different ways, taking into account consistency issues related to the SPH differential operators and using the projection of the Navier-Stokes equations on the solid boundary. It is shown that, when solid particles are considered, the energy equation of the particle system contains some extra-terms that depend on the pressure-velocity field extensions. The presence of these extra-terms does not affect the consistency of the SPH equation since they tend to vanish when the spatial resolution is increased. Two prototypical numerical test-cases are considered in order to give a quantitative description of this topic**

I. Introduction

The aim of the present work is to provide a further insight on the energy conservation in SPH schemes by considering the case of fluid-body interaction. Despite this topic includes a wide range of practical engineering applications (*e.g.* [1], [2], [3], [4]), it has been only partially addressed in the SPH literature: Randles and Libersky [5] and Bonet et al. [6] generalized the SPH energy equation in the context of the solid-mechanics, Monaghan [7] addressed the following topics: a) thermokinetic energy conservation, b) role of the time integrator on the energy conservation and c) boundary force derivation for treating fluid-solid interactions, and finally, Bouscasse et al. [8] discussed the ghost-fluid approach when used to simulate fluid-rigid body interactions.

A correct description of the energy exchanges between the fluid bulk and the solid structures is at the basis of a correct modelling of these problems. In SPH, a study on the energy conservation in the absence of solid bodies was carried out in its initial stages by *e.g.* Benz [9] and Hernquist & Katz [10]. A general structure of the energy equation (including the contributions from fluid-structure interactions) has been recently derived in [11], though the numerical examples provided in that work did not contain solid bodies.

The description of solid boundaries in SPH is a challenging problem and different approaches have been proposed over the years . On of these approaches is based on the fluid extension by the use of frozen/dummy particles, that is, particles placed in the solid domain, where the velocity, density and pressure fields should be imposed. Along this line, the simplest approach is setting the dummy particles velocity field identical to the body velocity, while the density and pressure fields derive from the continuity equation (e.g., [12], [13]). Slightly more complex field extensions are described in [14], [15] and [16], where the extended fluid fields are computed using the already available fluid data.

The techniques used to derive such extensions are the so-called mirroring procedures. About this topic, there exists a number of theoretical works that describe the properties of the different mirroring techniques (see, for example, [17], [18], [19]). As pointed out in [20], different extensions have to be considered for each SPH differential operator in order to ensure convergence and accuracy. As shown by Marrone et al. [21], the use of solid particles with proper mirroring techniques provides robust and reliable schemes.

The final step to model the solid-body interaction relies on the use of proper formulas for the computation of forces and momenta on the solid body [8].

In present paper, a theoretical analysis of the energy conservation properties of the SPH scheme, in the presence of solid boundaries, is undertaken. The theoretical framework fits with both dummy and ghost particle approaches even if, in the present case, only the latter approach is adopted for the application examples. It is shown that due to the approximations done during the mirroring stage some extra-terms appear in the energy equation. Two prototypical numerical test-cases are considered in order to give a quantitative description of this issue and to describe the behavior of such extra-terms as the spatial resolution increases.

II. A brief reference to the δ-SPH method

The analysis described in the present work is completely general and can be applied to a generic weakly-compressible SPH model. The derivation of the theoretical expressions has been carried out for the δ-SPH model [22]. The reason for choosing this variant is its widespread use by SPH practitioner,

due to the scheme's ability to reduce the high frequency oscillations of the pressure field. Using this scheme introduces an extra-term in the energy balances, which is accounted for in the derivations and that can be dropped if the classical SPH formulation were of interest. For the ease of the reader, a brief reference to such a scheme is reported. Equations for the δ-SPH model follow:

$$\begin{cases} \dfrac{\mathrm{d}\rho_i}{\mathrm{d}t} = -\rho_i \sum_j (\boldsymbol{u}_j - \boldsymbol{u}_i)\cdot\nabla_i W_{ij}\, V_j + \delta\, h\, c_0\, \mathcal{D}_i\,, \\ \dfrac{\mathrm{d}\boldsymbol{u}_i}{\mathrm{d}t} = -\dfrac{1}{\rho_i}\sum_j (p_j + p_i)\,\nabla_i W_{ij}\, V_j + \boldsymbol{g}_i + \dfrac{\mu}{\rho_i}\sum_j \pi_{ij}\,\nabla_i W_{ij}\, V_j\,, \\ \dfrac{\mathrm{d}\boldsymbol{r}_i}{\mathrm{d}t} = \boldsymbol{u}_i\,, \qquad p_i = c_0^2\,(\rho_i - \rho_0)\,, \qquad V_i = m_i/\rho_i\,. \end{cases} \tag{1}$$

where μ, c_0 and ρ_0 indicate respectively the dynamic viscosity, the selected speed of sound and the reference density; m_i, ρ_i, V_i, p_i, $\boldsymbol{u}_i$ and $\boldsymbol{r}_i$, are respectively the mass, the density, the volume, the pressure, the velocity and the position of the generic i-th particle. The vector $\boldsymbol{g}_i$ represents a generic body force acting on the i-th particle. W_{ij} is the kernel function and h is the smoothing length. In this work a Wendland C2 kernel function is used with a compact support with a radius equal to $2\,h$. The particles are initially set on a given distribution of points and are associated with an initial volume ΔV_{0j}. For instance, if a regular Cartesian lattice is used with a characteristic spacing Δx, we assign $\Delta V_{0j} = \Delta x^2$ for all the j particles. For a given initial density field ρ_{0j}, the mass of the particle is evaluated as: $m_j = \rho_{0j}\,\Delta V_{0j}$.

Unlike the particles' density and volume, their mass does not change in time. In the examples, the ratio $h/\Delta x$ is set equal to 2 which corresponds to a number of about 50 interacting neighbour particles in a 2D framework.

The diffusive term $\mathcal{D}_i$ and the viscous term π_{ij} in equation (1) are given by:

$$\begin{cases} \pi_{ij} := K\,\dfrac{(\boldsymbol{u}_j - \boldsymbol{u}_i)\cdot\boldsymbol{r}_{ji}}{\|\boldsymbol{r}_{ji}\|^2}\,, \\ \mathcal{D}_i := 2\sum_j \psi_{ji}\,\dfrac{\boldsymbol{r}_{ji}\cdot\nabla_i W_{ij}}{\|\boldsymbol{r}_{ji}\|^2}\,V_j\,, \qquad \boldsymbol{r}_{ji} := \boldsymbol{r}_j - \boldsymbol{r}_i, \\ \psi_{ji} := \left\{ \left(\rho_j - \rho_i\right) - \dfrac{1}{2}\left(\langle\nabla\rho\rangle_j^L + \langle\nabla\rho\rangle_i^L\right)\cdot\boldsymbol{r}_{ji} \right\}, \end{cases} \tag{2}$$

where $K = 2\,(n+2)$, n is the number of spatial dimensions and the symbol $\langle\nabla\rho\rangle_i^L$ indicates the renormalized density gradient (see [5] for more details).

As shown in [23], the parameter δ is not problem-dependent and its range of variation is quite narrow, Practically there is no need for a tuning and in the present work it has been set equal to 0.1 in all the simulations. The system (1) is integrated in time by using a fourth-order Runge-Kutta scheme.

In the following sections, we assume that the interaction with eventual solid structures is modelled through the use of ghost particles. These are briefly recalled in the next section.

A. Enforcement of the solid-boundary condition through a ghost-fluid method

In the present work the ghost-fluid technique is used to enforce the boundary conditions along the body surface. Specifically, the solid domain is modelled through a set of "fictitious particles" (hereinafter denoted as "ghost particles" and labelled with the subscript "g") and the velocity and pressure fields are extended on these particles through appropriate mirroring techniques. To this end, the solid surface is discretized in equispaced body nodes and a layer of ghost particles is disposed in the solid region. The ghost particle positions have been obtained by using the technique described in [15] and in [21]. The pressure/velocity fields assigned to the ghost particles, namely $(\boldsymbol{u}_g, p_g)$, are computed by using the values obtained at specific interpolation nodes internal to the fluid and uniquely associated with the fixed ghost particles. Hereinafter, the interpolated values are indicated through $(\boldsymbol{u}^*, p^*)$.

The pressure field p_g is mirrored on the ghost particles to enforce the following Neumann condition:

$$\frac{\partial p}{\partial \boldsymbol{n}} = \rho\left[\boldsymbol{g}\cdot\boldsymbol{n} - \frac{d\boldsymbol{u}_{\boldsymbol{B}}}{dt}\cdot\boldsymbol{n} + \nu\,\nabla^2\boldsymbol{u}\cdot\boldsymbol{n}\right], \tag{3}$$

where $\boldsymbol{u}_{\boldsymbol{B}}$ is the velocity of the solid boundary (for details see [15]). The last term is generally negligible for the Reynolds numbers considered in this work. This leads to:

$$p_g = p^* + \frac{\partial p}{\partial \boldsymbol{n}}\cdot(\boldsymbol{r}^* - \boldsymbol{r}_s)\,. \tag{4}$$

The velocity field for the ghost-fluid is subjected to a specific treatment. The ghost velocity $\boldsymbol{u}_g$ depends on both $\boldsymbol{u}^*$ and $\boldsymbol{u}_B$, the latter being the velocity of the nearest body node. [20] found that different mirroring techniques have to be used to evaluate the divergence operator in the continuity equation and the viscous term π_{ij}, to avoid inconsistencies and loss of accuracy. Generally, the mirroring techniques have to treat the components of $\boldsymbol{u}^*$ in the normal and tangential direction to the solid surface in a different way.

De Leffe et al. [20] proved that the velocity-divergence operator in (1) is convergent and consistent if the normal component of $\boldsymbol{u}^*$ is mirrored in the frame of reference of the solid profile, leaving the tangential component unaltered. Conversely, to evaluate the π_{ij} term, the velocity field has to be extended to approximate the no-slip conditions along the solid bodies. In this work, the normal component is left unaltered while the tangential component is set equal to the one of the body.

The consistency of such extension of the tangential component of the velocity field to compute the Laplacian was discussed in [17] where it was given the label U0M model. For practical applications such an extension procedure is proved to be sufficiently accurate if the spatial resolution of the boundary layer region is high enough (for details, see [16]). Incidentally, we recall that different mirroring procedures can be chosen to evaluate the viscous stresses. For a deeper discussion on this topic, we address the reader to [17], [24] and [19].

Summarising, we recall that:

1) the ghost-fluid fields $(p_g, \boldsymbol{u}_g)$ are functions of the interpolated fluid characteristics $(p^*, \boldsymbol{u}^*)$ as well as of the motion of the solid boundary $\boldsymbol{u}_B$
2) The ghost-fluid velocity used for the evaluation of the viscous term π_{ij} is, in general, different from the ghost velocity used in the continuity equation (the latter will be identified with the super-index C).

III. Energy Conservation in the SPH model

A. Energy Conservation equations at continuous level

In this section a general methodology to compute the energy components is discussed. The First law of Thermodynamics, i.e. the energy conservation, can be expressed as follows:

$$\frac{\mathrm{d}\mathcal{E}_M}{\mathrm{d}t} + \frac{\mathrm{d}\mathcal{E}_I}{\mathrm{d}t} = \mathcal{P}_{body/fluid} \tag{5}$$

where $\mathcal{E}_M$ and $\mathcal{E}_I$ are respectively the mechanical and internal energies of the fluid while $\mathcal{P}_{body/fluid}$ is the power delivered by the solid boundary $\partial\Omega_B$ on the fluid. The power $\mathcal{P}_{body/fluid}$ is obtained by integrating the elementary power acting on each surface element of $\partial\Omega_B$:

$$\mathcal{P}_{body/fluid} = \int_{\partial\Omega_B} \mathbb{T}\boldsymbol{n}_B \cdot \boldsymbol{u_B}\, dS \tag{6}$$

where $\boldsymbol{u_B}$ is the velocity of the body and $\boldsymbol{n}_B$ the normal unit vector pointing inward the solid body.

For a Newtonian fluid, the stress tensor reads:

$$\mathbb{T} = (-p + \lambda \,\mathrm{tr}\,\mathbb{D})\,\mathbb{I} + 2\mu\,\mathbb{D}, \tag{7}$$

where $\mathbb{D}$ is the rate of strain tensor, i.e. $\mathbb{D} = (\nabla\boldsymbol{u} + \nabla\boldsymbol{u}^T)/2$, and μ and λ are the viscosity coefficients. In the present work we assume the fluid to be weakly compressible and, consequently, the stress components related to the λ coefficient are neglected (see *e.g.* [25] and [26]). Using equation (7), we can split $\mathcal{P}_{body/fluid}$ in two components, one associated to the pressure field and the other with the viscous forces:

$$\mathcal{P}_{body/fluid} = \mathcal{P}^p_{body/fluid} + \mathcal{P}^V_{body/fluid},$$

$$\begin{cases} \mathcal{P}^p_{body/fluid} := \displaystyle\int_{\partial\Omega_B} \boldsymbol{u_B} \cdot \boldsymbol{dF}^p, \qquad \boldsymbol{dF}^p := -p\,\boldsymbol{n}_B\, dS, \\ \mathcal{P}^V_{body/fluid} := \displaystyle\int_{\partial\Omega_B} \boldsymbol{u_B} \cdot \boldsymbol{dF}^V, \qquad \boldsymbol{dF}^V := 2\mu\,\mathbb{D}\,\boldsymbol{n}_B\, dS, \end{cases} \tag{8}$$

being $\boldsymbol{dF}^p$ and $\boldsymbol{dF}^V$ the elementary pressure and viscous forces of the body surfaces acting on the fluid. Similarly to the previous decomposition, we write:

$$\boldsymbol{F}_{body/fluid} = \boldsymbol{F}^p_{body/fluid} + \boldsymbol{F}^V_{body/fluid},$$

$$\begin{cases} \boldsymbol{F}^p_{body/fluid} := \displaystyle\int_{\partial\Omega_B} \boldsymbol{dF}^p, \qquad \boldsymbol{dF}^p := -p\,\boldsymbol{n}_B\, dS, \\ \boldsymbol{F}^V_{body/fluid} := \displaystyle\int_{\partial\Omega_B} \boldsymbol{dF}^V, \qquad \boldsymbol{dF}^V := 2\mu\,\mathbb{D}\,\boldsymbol{n}_B\, dS, \end{cases} \tag{9}$$

where $\boldsymbol{F}_{body/fluid}$ is the total force applied by the body on the fluid and $\boldsymbol{F}^p_{body/fluid}$, $\boldsymbol{F}^V_{body/fluid}$ are the corresponding pressure and viscous components.

Under the assumption of weakly-compressibility, the constitutive equation for the internal energy $\mathcal{E}_I$ is:

$$\frac{\mathrm{d}\mathcal{E}_I}{\mathrm{d}t} = \frac{\mathrm{d}\mathcal{E}_C}{\mathrm{d}t} - \mathcal{P}_V \tag{10}$$

where $\mathcal{E}_C$ is the elastic energy due to the compressibility and $\mathcal{P}_V$ is the viscous dissipation (which is always negative in the theoretical model, consistently with the second law of Thermodynamics). Combining together equations (10) and (5), the First law of Thermodynamics becomes:

$$\frac{\mathrm{d}\mathcal{E}_M}{\mathrm{d}t} + \frac{\mathrm{d}\mathcal{E}_C}{\mathrm{d}t} - \mathcal{P}_V = \mathcal{P}^p_{body/fluid} + \mathcal{P}^V_{body/fluid}\,. \tag{11}$$

B. SPH evaluation of the fluid/solid force exchange through a ghost-fluid approach

Following the works [8], [16], the pressure and viscous components of the body force in the SPH model are expressed as:

$$\begin{aligned} \boldsymbol{F}^{p\ \mathrm{SPH}}_{body/fluid} &= -\sum_i^* \overline{\sum_j} V_i\, V_j \left(p_j + p_i\right) \nabla_i W_{ij} \\ \boldsymbol{F}^{V\ \mathrm{SPH}}_{body/fluid} &= \mu \sum_i^* \overline{\sum_j} V_i\, V_j\, \pi_{ij}\, \nabla_i W_{ij}\,. \end{aligned} \tag{12}$$

In the expression above, $\sum_i^*$ denotes the sum over the fluid particles and $\overline{\sum_j}$ denote the sum over the ghost particles inside the solid domain. Incidentally, we underline that the term $\sum_i^* \nabla_i W_{ij} V_i$ is a vector pointing inward the solid body (see *e.g.* [27]), similarly to the vector $\boldsymbol{n}_B$ in (9). This suggests a close analogy between the expressions in (12) and the theoretical contributions in (9). At the continuum, the proof of convergence of the SPH terms to the theoretical formulas is described in the appendix of [16].

As briefly explained in the section II-A, a ghost-fluid approach is here used to enforce the solid boundary condition. Therefore, a velocity field $\boldsymbol{u}_j$ (which is needed to estimate the term π_{ij}) and a pressure field p_j have to be properly defined in the solid domain. We recall that both $\boldsymbol{u}_j$ and p_j depend on the body motion (see section II-A) and that different mirroring procedures are necessary for the ghost velocity field used in the viscous stress π_{ij} and in the continuity equation (i.e., the first eq. of 1).

In analogy with equations (8) and (12), we evaluate the power that the solid particles apply on the fluid particles through the following formulae:

$$\begin{aligned} \mathcal{P}^{p\ \mathrm{SPH}}_{body/fluid} &= -\sum_i^* \overline{\sum_j} V_i\, V_j \left(p_j + p_i\right) \nabla_i W_{ij} \cdot \boldsymbol{u}_{Bj}, \\ \mathcal{P}^{V\ \mathrm{SPH}}_{body/fluid} &= \mu \sum_i^* \overline{\sum_j} V_i\, V_j\, \pi_{ij}\, \nabla_i W_{ij} \cdot \boldsymbol{u}_{Bj}, \end{aligned} \tag{13}$$

where $\boldsymbol{u}_{Bj}$ is the actual motion of the body at the position of the j-th fixed ghost particle, which can be different to the

extended fluid velocity field assigned to that ghost particle. It will be shown in the paper that such distinction needs to be clearly maintained in the SPH model in order to write, in a correct way, the energy conservation of the system.

C. SPH energy conservation equation

In the SPH model the kinetic and potential energies of the particle system are:

$$\mathcal{E}_K^{\text{SPH}}(t) = \frac{1}{2}\sum_i^* m_i \boldsymbol{u_i}^2, \qquad \mathcal{E}_P^{\text{SPH}}(t) = -\sum_i^* m_i \boldsymbol{g}\cdot\boldsymbol{r_i}. \quad (14)$$

The summation of the two contributions gives the mechanical energy, $\mathcal{E}_M^{\text{SPH}}$. The time variation of $\mathcal{E}_M^{\text{SPH}}$ is obtained by multiplying the SPH momentum equation by the particle velocity and rearranging (see [11] for details). This gives:

$$\begin{aligned}\frac{\mathrm{d}\mathcal{E}_M^{\text{SPH}}}{\mathrm{d}t} = &-\sum_i^*\sum_j V_i V_j \left(p_j + p_i\right)\boldsymbol{u}_i\cdot\nabla_i W_{ij} \\ &+\mu\sum_i^*\sum_j V_i V_j \pi_{ij}\boldsymbol{u}_i\cdot\nabla_i W_{ij}, \end{aligned} \quad (15)$$

where $\sum_j$ denotes the sum over both the fluid and the ghost particles.

A further rearrangement of equation 15 (see [11] for details) allows one to derive the final equation for the energy balance of the SPH fluid particle system:

$$\frac{\mathrm{d}\mathcal{E}_M^{\text{SPH}}}{\mathrm{d}t} + \frac{\mathrm{d}\mathcal{E}_C^{\text{SPH}}}{\mathrm{d}t} - (\mathcal{P}_\delta + \mathcal{P}_V^{\text{SPH}}) = \mathcal{P}_s^V + \mathcal{P}_s^p + \mathcal{P}_s^C,$$

$$\left\{\begin{array}{lcl} \mathcal{P}_\delta & := & -\delta h c_0 \sum_i^* \frac{p_i}{\rho_i}\mathcal{D}_i V_i, \\ \mathcal{P}_V^{\text{SPH}} & := & -\frac{\mu}{2}\sum_i^*\sum_j^* V_i V_j \pi_{ij}\left(\boldsymbol{u}_j - \boldsymbol{u}_i\right)\cdot\nabla_i W_{ij}, \\ \mathcal{P}_s^V & := & \mu\sum_i^*\sum_j^{\overline{\ }} V_i V_j \pi_{ij}\boldsymbol{u}_i\cdot\nabla_i W_{ij}, \\ \mathcal{P}_s^p & := & -\sum_i^*\sum_j^{\overline{\ }} V_i V_j \left(p_j + p_i\right)\boldsymbol{u}_i\cdot\nabla_i W_{ij}, \\ \mathcal{P}_s^C & := & -\sum_i^*\sum_j^{\overline{\ }} V_i V_j p_i \left(\boldsymbol{u}_j^C - \boldsymbol{u}_i\right)\cdot\nabla_i W_{ij}. \end{array}\right. \quad (16)$$

In these formulae, the subindex s is reserved for the terms related to the fluid energy variation rates due to the interaction with the solid boundary. The meaning of each term is:

- $\mathcal{P}_\delta$ represents the power of the diffusive term of the δ-SPH scheme [11],
- $\mathcal{P}_V^{\text{SPH}}$ is the SPH discretization of the viscous dissipation $\mathcal{P}_V$,
- $\mathcal{P}_s^V$ is the mechanical power transferred from the solid to the liquid particles through viscous diffusion,
- $\mathcal{P}_s^p$ is the mechanical power transferred from the solid to the liquid particles through pressure forces, and
- $\mathcal{P}_s^C$ is an spurious numerical compressible power depending on the difference between the extended and fluid velocity fields.

In equation (16), since $\mathcal{P}_\delta$ represents a numerical dissipation, it is combined with $\mathcal{P}_V^{\text{SPH}}$ and moved to the left-hand side.

The term $\mathcal{P}_s^C$ is related to the compressibility of the fluid and, therefore, it should be negligible in the weakly compressible regime. For a flat solid surface (where the classical ghost approach can be used, e.g. [28]), this term is zero by construction. Conversely, for more complex geometries this is in general not true and this term should be monitored during numerical simulations.

Comparing equations (16) and equations (11), a close relation between $\mathcal{P}^{p\ \text{SPH}}_{body/fluid}$, $\mathcal{P}^{V\ \text{SPH}}_{body/fluid}$ and the power $\mathcal{P}_s := \mathcal{P}_s^V + \mathcal{P}_s^p + \mathcal{P}_s^C$ arises:

$$\mathcal{P}_s^V + \mathcal{P}_s^p + \mathcal{P}_s^C = \mathcal{P}^{V\ \text{SPH}}_{body/fluid} + \mathcal{P}^{p\ \text{SPH}}_{body/fluid} + \Delta\mathcal{P}^V + \Delta\mathcal{P}^p + \Delta\mathcal{P}^C, \quad (17)$$

where the expressions for the terms $\Delta\mathcal{P}^V$, $\Delta\mathcal{P}^p$ and $\Delta\mathcal{P}^C$ are:

$$\left\{\begin{array}{lcl} \Delta\mathcal{P}^V & := & \mu\sum_i^*\sum_j^{\overline{\ }} V_i V_j \pi_{ij}\left(\boldsymbol{u}_i - \boldsymbol{u}_j\right)\cdot\nabla_i W_{ij} \\ \Delta\mathcal{P}^p & := & -\sum_i^*\sum_j^{\overline{\ }} V_i V_j \left(p_j + p_i\right)\left(\boldsymbol{u}_i - \boldsymbol{u}_{Bj}\right)\cdot\nabla_i W_{ij} \\ \Delta\mathcal{P}^C & := & \sum_i^*\sum_j^{\overline{\ }} V_i V_j p_i \left(\boldsymbol{u}_i - \boldsymbol{u}_j^C\right)\cdot\nabla_i W_{ij}. \end{array}\right. \quad (18)$$

It should be noticed again that π_{ij}, p_j and $\boldsymbol{u}_j^C$ depend on the specific mirroring/extension model applied.

Using the above notation the SPH energy conservation equation can be rewritten as:

$$\frac{\mathrm{d}\mathcal{E}_M^{\text{SPH}}}{\mathrm{d}t} + \frac{\mathrm{d}\mathcal{E}_C^{\text{SPH}}}{\mathrm{d}t} - \mathcal{P}_V^{\text{SPH}} - \left(\mathcal{P}_\delta + \Delta\mathcal{P}^V + \Delta\mathcal{P}^p + \Delta\mathcal{P}^C\right) = \mathcal{P}^{V\ \text{SPH}}_{body/fluid} + \mathcal{P}^{p\ \text{SPH}}_{body/fluid}, \quad (19)$$

where the terms in brackets in the left hand-side have to converge to zero for consistency in the limit $(\Delta x/L, \Delta x/h) \to 0$. For the terms $\Delta\mathcal{P}^V$, $\Delta\mathcal{P}^p$, this is achieved since $\boldsymbol{u}_i$ has to tend to $\boldsymbol{u}_{Bj}$ within the same limit for a proper enforcement of the no-slip boundary condition.

In the following section two test cases are considered in order determine the signs, the sizes and the convergence rates of the three different power components, namely $\Delta\mathcal{P}^V$, $\Delta\mathcal{P}^p$ and $\Delta\mathcal{P}^C$. For what concerns P_δ, in [11] it is shown that this term is negative and converge to zero when increasing the spatial resolution. Since $\Delta\mathcal{P}^V$, $\Delta\mathcal{P}^p$ and $\Delta\mathcal{P}^C$ are affected by the choice of the specific ghost-fluid field, the present analysis can be regarded as an alternative approach to study the consistency of the mirroring procedures with respect to previous works [17], [24], [19], [18].

The different power components are integrated in time as

follows:

$$\mathcal{E} := \mathcal{E}_0 + \int_0^t \mathcal{E}\, dt\,, \qquad \Delta\mathcal{E} := \mathcal{E} - \mathcal{E}_0,$$
$$Q_V := -\int_0^t \mathcal{P}_V\, dt\,, \qquad Q_\delta := -\int_0^t \mathcal{P}_\delta\, dt,$$
$$\mathcal{W}_s := \int_0^t \mathcal{P}_s\, dt\,, \qquad \mathcal{W}_{body/fluid} := \int_0^t \mathcal{P}_{body/fluid}\, dt, \tag{20}$$

where the superscript SPH has been removed for the sake of simplicity. A positive sign for the heats Q means that the fluid system is losing mechanical energy and is increasing its internal energy. Similarly, a positive sign for the works $\mathcal{W}$ means that the body is doing work on the fluid. According to equation (19), the energy conservation in the time interval $[0, t]$ is given by:

$$\mathcal{E}_M + \mathcal{E}_C + Q_V - \mathcal{W}_{body/fluid} + (Q_\delta - \Delta\mathcal{W}) = \mathcal{E}_{M0} + \mathcal{E}_{C0},$$
$$\mathcal{W}_{body/fluid} := \mathcal{W}^p_{body/fluid} + \mathcal{W}^V_{body/fluid},$$
$$\Delta\mathcal{W} := \int_0^t \left(\Delta\mathcal{P}^V + \Delta\mathcal{P}^p + \Delta\mathcal{P}^C\right) dt = \mathcal{W}_s - \mathcal{W}_{body/fluid}. \tag{21}$$

On one hand, $\mathcal{W}_{body/fluid}$ can be interpreted as the "nominal" mechanical work done by the solid particles on the fluid ones, computed by integrating in time (eq. 20) the power obtained with particle summations (eq. 13). On the other hand, $\mathcal{W}_s$ is the effective mechanical work done by the solid particles on the fluid ones, globally computed from the SPH energy balance (eq. 21).

Along with Q_δ (which, in any case, is a numerical term), it can be demonstrated that $\Delta\mathcal{P}^V$ is always zero or negative if the U0M model extension (the ghost particle is assigned the solid velocity at the ghost particle position - see [17] for details) is used to compute the velocity Laplacian and conjecture, based on the results of the numerical experiments in the following section, that $\Delta\mathcal{W}$ is always negative under the same conditions.

IV. Numerical test-cases

A. Moving circular cylinder in a viscous fluid

In the first test case a circular cylinder moving with the time law described in Figure 1 is considered. After the acceleration phase, the body moves inside the rectangular domain with an uniform rectilinear motion. The time interval is $tU/D \in [0, 18]$, where D is the cylinder diameter. At the final instant (namely, $tU/D = 18$) the body approaches the right wall of the domain but is still far enough not to be influenced by it. The Reynolds number is $\mathrm{Re} = UD/\nu = 200$. For δ-SPH the flow around a circular cylinder with this Reynolds number has been already validated by [16].

Figure 2 depicts the main flow features through the use of passive Lagrangian trackers. The wake shed by the cylinder is remarkable and, because of the relatively short time of the evolution, it remains practically symmetric with respect to the centerline $y = 2.5D$. The spatial resolution is $D/\Delta x = 200$, involving about 4 million particles.

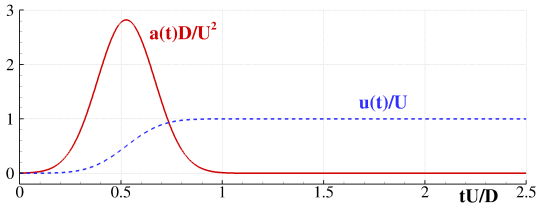

Fig. 1. Moving circular cylinder: time law of motion.

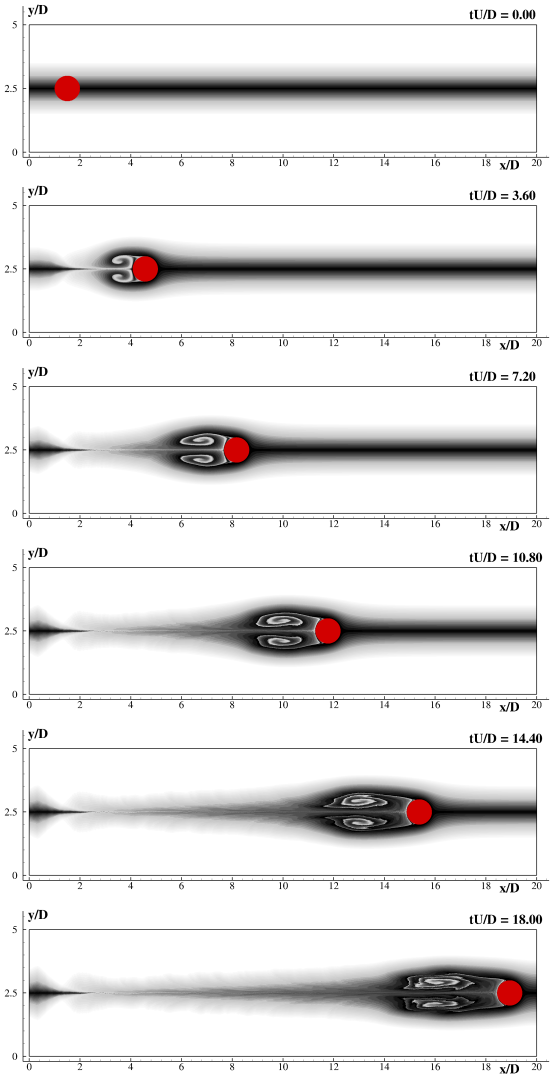

Fig. 2. Moving circular cylinder: time evolution of lagrangian trackers (Re=200 and $D/\Delta x = 200$).

Figure 3 reports the time histories of the mechanical power $d\mathcal{E}_M\,/\,dt$, the elastic/compressible power $d\mathcal{E}_C\,/\,dt$, the viscous dissipation $\mathcal{P}_V$ and the dissipation due to the numerical diffusion $\mathcal{P}_\delta$. The latter is practically negligible and, therefore, will be ignored in the energy balance.

In Figure 4, the power terms associated with the pressure and the weakly-compressibility assumption are displayed. The nominal fluid/body pressure power $\mathcal{P}^p_{fluid/body}$ is practically

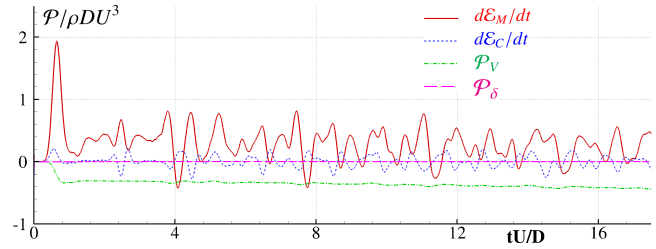

Fig. 3. Moving circular cylinder: time evolution of the different power components (Re=200 and $D/\Delta x = 200$).

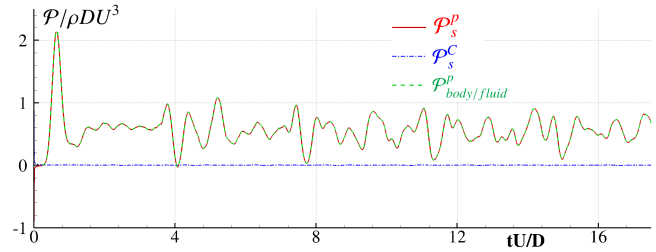

Fig. 4. Moving circular cylinder: time evolution of the power components $\mathcal{P}^p_s$, $\mathcal{P}^C_s$ and $\mathcal{P}^p_{body/fluid}$ (Re=200 and $D/\Delta x = 200$).

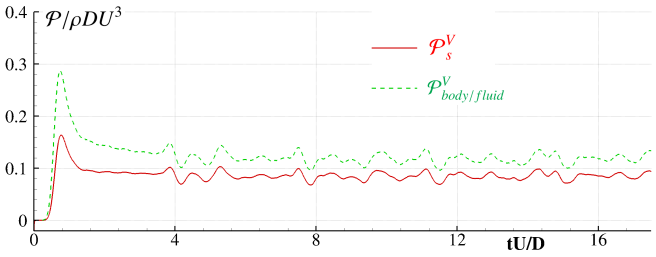

Fig. 5. Moving circular cylinder: time evolution of the power components $\mathcal{P}^V_s$ and $\mathcal{P}^V_{body/fluid}$ (Re=200 and $D/\Delta x = 200$).

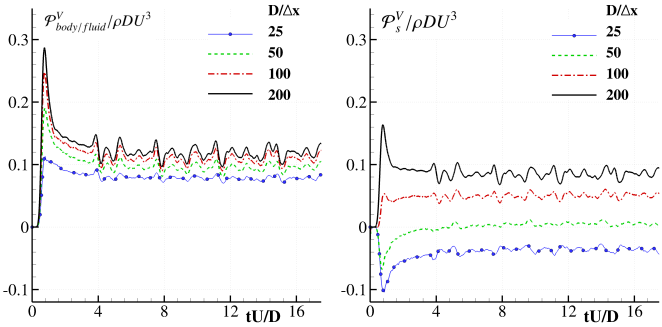

Fig. 6. Moving circular cylinder: time evolution of the power $\mathcal{P}^V_{body/fluid}$ (left) and $\mathcal{P}^V_s$ (right) components as the spatial resolution increases (Re=200).

superimposed to the effective pressure power $\mathcal{P}^p_S$ while the compressible power $\mathcal{P}^C_s$ is practically negligible with respect the other two components.

On the contrary, a non negligible discrepancy appears in the viscous components $\mathcal{P}^V_s$ and $\mathcal{P}^V_{body/fluid}$ (see Figure 5). In this

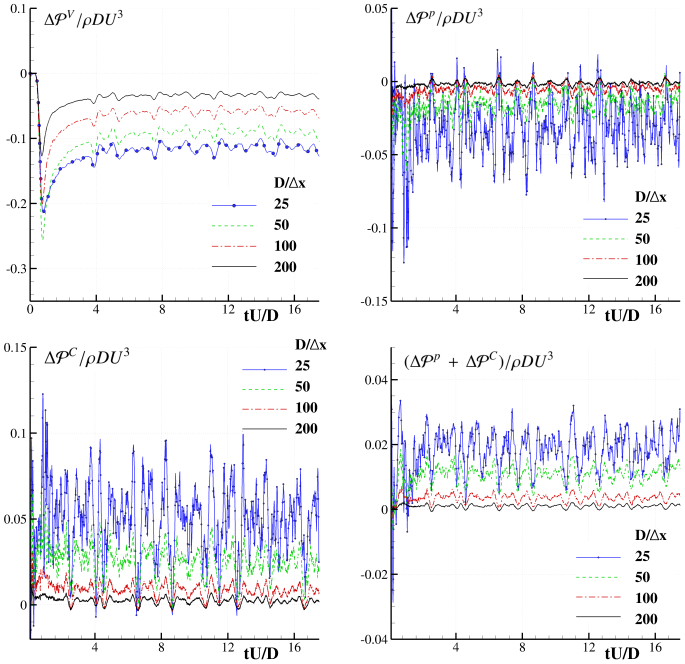

Fig. 7. Moving circular cylinder: time evolution of the power terms $\Delta\mathcal{P}^V$, $\Delta\mathcal{P}^p$, $\Delta\mathcal{P}^C$ and $(\Delta\mathcal{P}^p + \Delta\mathcal{P}^C)$ as the spatial resolution increases (Re=200).

case the nominal power $\mathcal{P}^V_{body/fluid}$ is significantly higher than the effective power $\mathcal{P}^V_s$. This issue is not due to an insufficient discretization of the fluid domain. Indeed, the adopted spatial resolution (i.e, $D/\Delta x = 200$) is sufficiently high for simulating a viscous flow with Re = 200 (see [16])

The results displayed in Figure 6 give a deeper inspection of such inconsistency in the energy balance of the viscous terms. The left plot shows the time evolution of the nominal power $\mathcal{P}^V_{body/fluid}$ by increasing the spatial resolution. In accordance with [16], the differences between $D/\Delta x = 100$ and $D/\Delta x = 200$ are not large, even if they are not negligible yet. On the contrary, the effective power $\mathcal{P}^V_s$ shows poor convergence (right plot of figure 6). This suggests that $\mathcal{P}^V_s$ requires a very high spatial resolution to converge to the nominal power $\mathcal{P}^V_{body/fluid}$. Figure 7 shows the time histories of the power terms $\Delta\mathcal{P}^V$, $\Delta\mathcal{P}^p$ and $\Delta\mathcal{P}^C$ as the spatial resolution increases. In accordance with the consistency issue discussed in section III-C, all terms decrease when Δx decreases. In particular, $\Delta\mathcal{P}^p$ and $\Delta\mathcal{P}^C$ are opposite in sign and, consequently, the sum $\Delta\mathcal{P}^p + \Delta\mathcal{P}^C$ is smaller in magnitude than the two separate components (right-bottom plot of figure 7). Note that this sum has a positive sign during the largest part of the evolution. The convergence rate of $\Delta\mathcal{P}^p$ and $\Delta\mathcal{P}^C$ is about 1 and their magnitudes are practically negligible with respect to $\mathcal{P}^p_{fluid/body}$ and $\mathcal{P}^p_S$. On the contrary, $\Delta\mathcal{P}^V$ is not negligible in comparison to $\mathcal{P}^V_s$ and its rate of convergence is about 0.4 for the coarsest resolution while it increases to about 1 for the two highest resolutions.

Finally, figure 8 shows the time histories of the different energy components: (i) the mechanical energy $\Delta\mathcal{E}_M$, (ii) the elastic/compressible energy $\Delta\mathcal{E}_C$, (iii) the viscous dissipation

Q_V, (iv) the nominal work exerted by the solid particle $W_{body/fluid}$ and (v) the effective work exerted by the solid particle $\mathcal{W}_s$. The difference $\Delta\mathcal{W} = (\mathcal{W}_{body/fluid} - \mathcal{W}_s)$ is the positive extra numerical work. Even when the resolution is relatively fine (e.g. $D/\Delta x = 200$), this term remains sensibly different from zero.

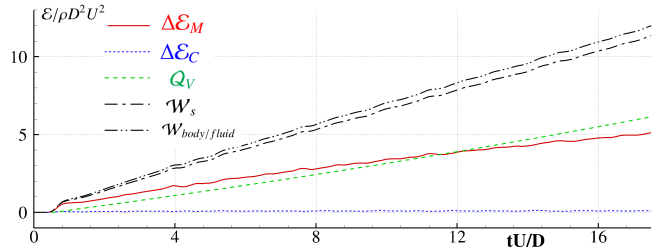

Fig. 8. Moving circular cylinder: time evolution of the different energy components (Re=200 and $D/\Delta x = 200$).

B. Unsteady viscous flow around an elliptical cylinder

In the second test case an inclined elliptical cylinder that moves with a similar time law, but differently from the previous test-case, both an acceleration and a braking stage are considered. The main flow features are described in Figure 9 where the complex, non-symmetric behavior of the wake shed by the cylinder is highlighted through the time evolution of passive Lagrangian trackers. The Reynolds number is $\mathrm{Re} = UD/\nu = 200$ where D is the ellipse major axis. For the δ-SPH method, the flow around the same geometry at a more challenging Reynolds number equal to 500 has been validated in [29]. As for previous test-case, the maximum spatial resolution adopted is $D/\Delta x = 200$.

The convergence of the viscous power terms $\mathcal{P}^V_{body/fluid}$ and $\mathcal{P}^V_s$ is sketched in figure 10. Like the previous test-case, the nominal power $\mathcal{P}^V_{body/fluid}$ converges much faster than the effective one, namely $\mathcal{P}^V_s$. Remarkably, we observe that at time $tU/D = 19$ the cylinder has stopped and, therefore, $\mathcal{P}^V_{body/fluid}$ is practically zero for $tU/D > 19$. On the contrary, a short transitory is needed before $\mathcal{P}^V_s$ goes to zero.

Finally, Figure 11 sketches the time histories of the different energy components involved in eq. (16). The difference $\Delta\mathcal{W} = (\mathcal{W}_{body/fluid} - \mathcal{W}_s)$ (i.e., the difference between the nominal and effective works exerted by the body on the fluid) is, as for previous case, a positive non-negligible extra term.

Conclusions

The energy conservation of SPH method has been studied in the occurrence of fluid-solid interactions. The solid bodies have been modeled through solid particles so that the whole solid-fluid domain has been described as a unique particle system. Suitable extensions of the pressure and velocity fields have been defined on the solid particles in order to enforce the solid boundary condition in a consistent way.

It has been demonstrated that, when solid particles are considered, the energy equation of the particle system contains

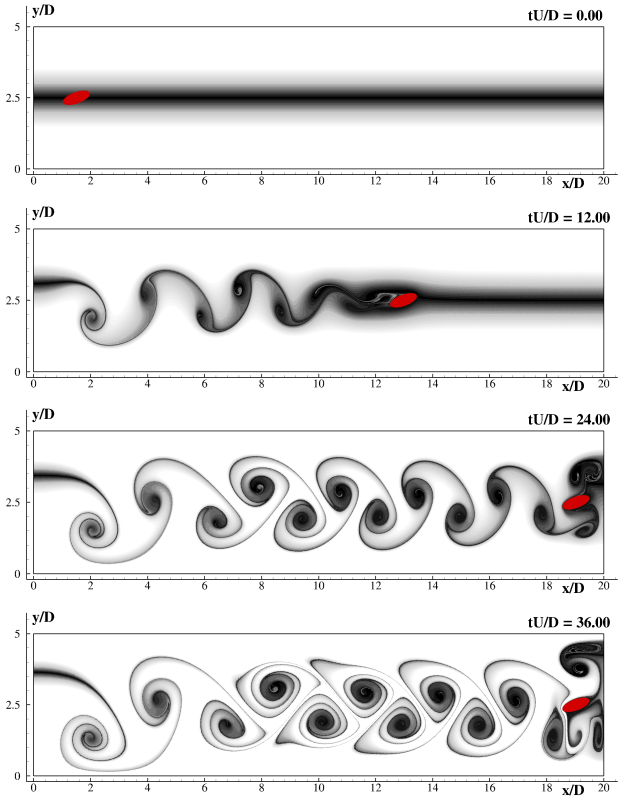

Fig. 9. Elliptical cylinder: Lagrangian trackers (Re=200 and $D/\Delta x = 200$).

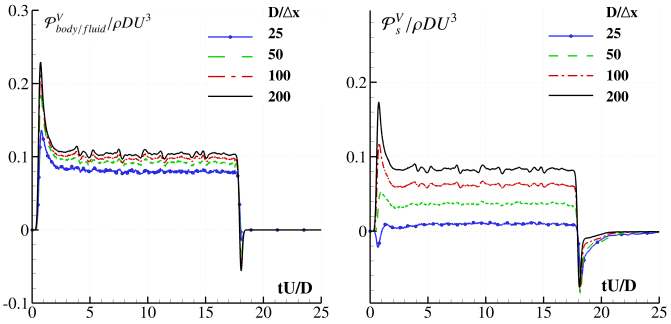

Fig. 10. Unsteady viscous flow around an elliptical cylinder. Time evolution of the power $\mathcal{P}^V_{body/fluid}$ (left) and $\mathcal{P}^V_s$ (right) components varying the spatial resolution $D/\Delta x$ (see eq. 16, 13, Re=200).

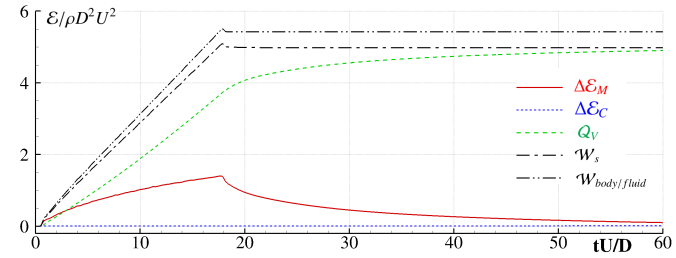

Fig. 11. Unsteady viscous flow around an elliptical cylinder: time evolution of the different energy components (see eq. 16, Re=200 and $D/\Delta x = 200$).

some extra-terms that depend on the pressure-velocity field extensions. For the extensions proposed in this work, those extra-terms do not affect the consistency of the SPH equation since they diminish when the spatial resolution is increased. However, the magnitudes of these extra-terms are affected by the choice of the specific ghost-fluid field and, consequently, the present analysis can be also regarded as an alternative approach to study the consistency of the pressure-velocity extensions. The extra terms are due to the difference between the *nominal* work done by the solid particles on the fluid particles and the *effective* one (i.e., the work directly derived from the SPH energy balance). It is conjectured in the paper that this extra term leads to extra dissipation.

Two numerical test-cases have been considered in order to determine the magnitude and convergence rates of the extra power terms. Both test-cases include a solid body moving through a viscous flow inside a confined domain with a prescribed time law. In the first test case a circular cylinder is considered while in the second one an elliptical profile with a non-null angle of attack is studied. In the latter case, both an initial acceleration and a final braking phase are described. In fact, when the body stops, the extra power terms are not null and decay to zero only after a transitory stage. In both test-cases the difference between the nominal and effective work, $\Delta\mathcal{W}$, is always negative and, therefore, can be regarded as a non-negligible extra-dissipation term.

Acknowledgements

Work supported by the Flagship Project RITMARE - Italian Research for the Sea - coordinated by Italian National Research Council and funded by Italian Ministry of Education, University and Research within Nat. Res. Program 2015-2016. and, on the Spanish side, by Spanish Ministry for Economy and Competitiveness under grants TRA2013-41096-P and ENE2014-59194-C2-2-R.

References

[1] G. Oger, M. Doring, B. Alessandrini, and P. Ferrant, "Two-dimensional SPH simulations of wedge water entries," *J. Comp. Phys.*, vol. 213 (2), pp. 803–822, 2006.

[2] R. Vacondio, B. Rogers, P. Stansby, P. Mignosa, and J. Feldman, "Variable resolution for SPH: a dynamic particle coalescing and splitting scheme," *Comp. Meth. in App. Mech. and Eng.*, 2013.

[3] A. Amicarelli, R. Albano, D. Mirauda, G. Agate, A. Sole, and R. Guandalini, "A Smoothed Particle Hydrodynamics model for 3D solid body transport in free surface flows," *Computers and Fluids*, vol. 116, pp. 205–228, 2015.

[4] R. B. Canelas, A. J. Crespo, J. M. Domínguez, R. M. Ferreira, and M. Gómez-Gesteira, "SPH-DCDEM model for arbitrary geometries in free surface solid-fluid flows," *Comp. Phys. Comm.*, pp. –, 2016.

[5] P. Randles and L. Libersky, "Smoothed Particle Hydrodynamics: some recent improvements and applications," *Computer methods in applied mechanics and engineering*, vol. 39, pp. 375–408, 1996.

[6] J. Bonet, S. Kulasegaram, M. Rodriguez-Paz, and M. Profit, "Variational formulation for the smooth particle hydrodynamics (SPH) simulation of fluid and solid problems," *Computer Methods in Applied Mechanics and Engineering*, vol. 193, no. 12–14, pp. 1245–1256, 2004, meshfree Methods: Recent Advances and New Applications.

[7] J. J. Monaghan, "Smoothed particle hydrodynamics," *Reports on Progress in Physics*, vol. 68, pp. 1703–1759, 2005.

[8] B. Bouscasse, A. Colagrossi, S. Marrone, and M. Antuono, "Nonlinear water wave interaction with floating bodies in SPH," *Journal of Fluids and Structures*, vol. 42, pp. 112–129, 2013.

[9] W. Benz, "Smooth Particle Hydrodynamics: A Review," *Harvard-Smithsonian Center for Astrophysics*, vol. Preprint No. 2884, 1989.

[10] L. Hernquist and N. Katz, "TreeSPH: A Unification of SPH with the Hierarchical Tree Method," *Astrophysical Journal Supplement*, vol. 70, pp. 419–446, 1989.

[11] M. Antuono, S. Marrone, A. Colagrossi, and B. Bouscasse, "Energy balance in the δ-SPH scheme," *Computer Methods in Applied Mechanics and Engineering*, vol. 289, pp. 209–226, 2015.

[12] R. Issa, E. S. Lee, D. Violeau, and D. R. Laurence, "Incompressible separated flows simulations with the smoothed particle hydrodynamics gridless method," *International journal for numerical methods in fluids*, vol. 47, no. 10-11, pp. 1101–1106, 2005.

[13] A. Crespo, M. Gómez-Gesteira, and R. A. Dalrymple, "Boundary conditions generated by dynamic particles in SPH methods," *CMC-TECH SCIENCE PRESS-*, vol. 5, no. 3, p. 173, 2007.

[14] D. Violeau and R. Issa, "Numerical modelling of complex turbulent free surface flows with the SPH Lagrangian method: an overview," *Int. J. Num. Meth. Fluids*, vol. 53(2), pp. 277–304, 2006.

[15] S. Marrone, M. Antuono, A. Colagrossi, G. Colicchio, D. Le Touzé, and G. Graziani, "Delta-SPH model for simulating violent impact flows," *Computer Methods in Applied Mechanics and Engineering*, vol. 200, no. 13-16, pp. 1526–1542, 2011.

[16] S. Marrone, A. Colagrossi, M. Antuono, G. Colicchio, and G. Graziani, "An accurate SPH modeling of viscous flows around bodies at low and moderate Reynolds numbers," *Journal of Computational Physics*, vol. 245, pp. 456–475, 2013.

[17] F. Macià, M. Antuono, L. M. González, and A. Colagrossi, "Theoretical Analysis of the No-Slip Boundary Condition Enforcement in SPH Methods," *Progress of Theoretical Physics*, vol. 125, no. 6, pp. 1091–1121, 2011. [Online]. Available: http://ptp.ipap.jp/link?PTP/125/1091/

[18] P. Merino-Alonso, F. Macia, A. Souto-Iglesias, and A. Colagrossi, "Consistency analysis of flow field extension models into ghost fluid regions for SPH solid body boundary condition implementations," in *8th SPHERIC workshop on SPH applications*, 2013, pp. 23–29.

[19] A. Souto-Iglesias, L. M. González, A. Colagrossi, and M. Antuono, "SPH no-slip BC implementation analysis at the continuous level," in *5th SPHERIC workshop on SPH applications*, 2010, pp. 29–36.

[20] M. De Leffe, D. Le Touzé, and B. Alessandrini, "A modified no-slip condition in weakly-compressible SPH," in *6th ERCOFTAC SPHERIC workshop on SPH applications*, 2011, pp. 291–297.

[21] S. Marrone, A. Colagrossi, M. Antuono, C. Lugni, and M. Tulin, "A 2D+t SPH model to study the breaking wave pattern generated by fast ships," *Journal of Fluids & Str.*, vol. 27, no. 8, pp. 1199–1215, 2011.

[22] M. Antuono, A. Colagrossi, S. Marrone, and D. Molteni, "Free-surface flows solved by means of SPH schemes with numerical diffusive terms," *Computer Physics Communications*, vol. 181, no. 3, pp. 532–549, 2010.

[23] M. Antuono, A. Colagrossi, and S. Marrone, "Numerical diffusive terms in weakly-compressible SPH schemes," *Computer Physics Communications*, vol. 183, no. 12, pp. 2570–2580, 2012.

[24] A. Colagrossi, L. Delorme, G. Colicchio, A. Souto-Iglesias, and J. L. Cercós-Pita, "Reynolds number and Shallow Depth Sloshing," in *3rd SPHERIC workshop on SPH applications*, June, 4-6 2008, pp. 221–228.

[25] A. Colagrossi, M. Antuono, A. Souto-Iglesias, and D. Le Touzé, "Theoretical analysis and numerical verification of the consistency of viscous smoothed-particle-hydrodynamics formulations in simulating free-surface flows," *Physical Review E*, vol. 84, p. 026705, 2011.

[26] A. Colagrossi, A. Souto-Iglesias, M. Antuono, and S. Marrone, "Smoothed-particle-hydrodynamics modeling of dissipation mechanisms in gravity waves," *Phys. Rev. E*, vol. 87, p. 023302, 2013.

[27] A. Colagrossi, B. Bouscasse, M. Antuono, and S. Marrone, "Particle packing algorithm for SPH schemes," *Computer Physics Communications*, vol. 183, no. 2, pp. 1641–1683, 2012.

[28] A. Colagrossi and M. Landrini, "Numerical Simulation of Interfacial Flows by Smoothed Particle Hydrodynamics," *J. Comp. Phys.*, vol. 191, pp. 448–475, 2003.

[29] E. Rossi, A. Colagrossi, B. Bouscasse, and G. Graziani, "The Diffused Vortex Hydrodynamics method," *Communications in Computational Physics*, vol. 18, no. 2, pp. 351–379, 2015.